Atomistic calculations of dislocation core energy in aluminium

X. W. Zhou,[1,*] R. B. Sills,[2] D. K. Ward,[3] and R. A. Karnesky[4]

[1]*Mechanics of Materials Department, Sandia National Laboratories, Livermore, California 94550, USA*

[2]*Gas Transfer Systems Department, Sandia National Laboratories, Livermore, California 94550, USA*

[3]*Radiation and Nuclear Detection Materials and Analysis Department, Sandia National Laboratories, Livermore, California 94550, USA*

[4]*Hydrogen and Materials Science Department, Sandia National Laboratories, Livermore, California 94550, USA*

(Received 29 February 2016; revised manuscript received 23 January 2017; published 16 February 2017)

A robust molecular-dynamics simulation method for calculating dislocation core energies has been developed. This method has unique advantages: It does not require artificial boundary conditions, is applicable for mixed dislocations, and can yield converged results regardless of the atomistic system size. Utilizing a high-fidelity bond order potential, we have applied this method in aluminium to calculate the dislocation core energy as a function of the angle β between the dislocation line and the Burgers vector. These calculations show that, for the face-centered-cubic aluminium explored, the dislocation core energy follows the same functional dependence on β as the dislocation elastic energy: $E_c = A\sin^2\beta + B\cos^2\beta$, and this dependence is independent of temperature between 100 and 300 K. By further analyzing the energetics of an extended dislocation core, we elucidate the relationship between the core energy and the core radius of a perfect versus an extended dislocation. With our methodology, the dislocation core energy can accurately be accounted for in models of dislocation-mediated plasticity.

DOI: 10.1103/PhysRevB.95.054112

I. INTRODUCTION

With low hydrogen solubility and a high strength-to-weight ratio, aluminium alloys are attractive for both hydrogen energy and transportation applications, respectively, that require high resistance to hydrogen embrittlement and light weight. Dislocation dynamics (DD) simulations [1] provide a tool for studying the mechanical properties of metals and alloys. One key input for DD simulations that is often overlooked is the core energy of dislocation lines and its variation with the character angle β formed between the line and the Burgers vector. The core energy contributes to the dislocation line tension and alters the behavior of dislocation lines as they bow out to bypass obstacles and react to form junctions. Unfortunately, dislocation cores cannot be described by linear elasticity theory, and hence their study requires a computational tool with atomistic resolution. Despite the pioneering work by Cai *et al.* [2,3] and Li *et al.* [4], much remains poorly understood concerning the nature of dislocation cores and their energies.

Dislocation core energies can be calculated using quantum-mechanical or empirical atomistic simulations under continuum [5–8], free [9], or periodic [1–4,10–15] boundary conditions. Continuum boundary conditions are challenging to use when dislocation configurations are unknown *a priori*, such as in face-centered-cubic (fcc) metals (e.g., aluminium) where perfect dislocations dissociate into partial dislocations separated by a stacking fault. Periodic boundary conditions usually are implemented using a so-called quadruple dislocation configuration [10] where positive and negative dislocations (lying in z) alternate in sign in both the x and the y directions so that a negative dislocation can recover the crystal periodicity destroyed by the preceding positive dislocation in both x and y directions. Although the quadruple configuration requires an orthorhombic computational cell to include four dislocations, it can be replicated with a nonorthorhombic cell containing only two dislocations [10,16]. A potential difficulty with this method is that, because positive and negative dislocations are on the same slip plane (x direction), they can glide and annihilate. This configuration cannot be used unless a barrier, such as the Peierls stress is sufficiently strong to pin the dislocations in place. A more general dislocation configuration that enables an offset of dislocations on different slip planes may solve this problem [2–4,16]. Dislocation core energies of aluminium have also been calculated using the generalized stacking fault energy obtained from density functional theory [17]. Because core relaxation is not treated directly in this model, however, it is unclear how this method compares with the direct atomistic simulation approach.

Recently, we have used molecular dynamics (MD) to calculate core energies of edge dislocations under periodic boundary conditions [18]. In our approach, we eliminate the alternation of dislocations in x, which prevents annihilation by glide. The purpose of the present paper is threefold: (a) Further extend this method to mixed dislocations and generate a complete set of aluminium dislocation core energies over the full range of possible character angles; (b) establish a generic analytical equation for the dislocation core energy in aluminium; and (c) further our understanding of the physics of dislocation cores in fcc metals. For our calculations, we utilize a high-fidelity Al-Cu bond order potential [19].

II. METHODS

The overall approach we will use for computing the core energy is similar to the other methods discussed above. Using atomistic simulations, we will compute the total energy per unit length of dislocation Γ of a multipolar dislocation system. This line energy can be expressed in terms of two contributions as

$$\Gamma(\beta) = E_c(\beta) + E_{el}(\beta), \tag{1}$$

where E_c and E_{el}, respectively, are the core and elastic energies per unit length of the dislocation and β is the character angle. Using elasticity theory, the elastic energy can be computed analytically in isotropic theory [18] and numerically using

*xzhou@sandia.gov

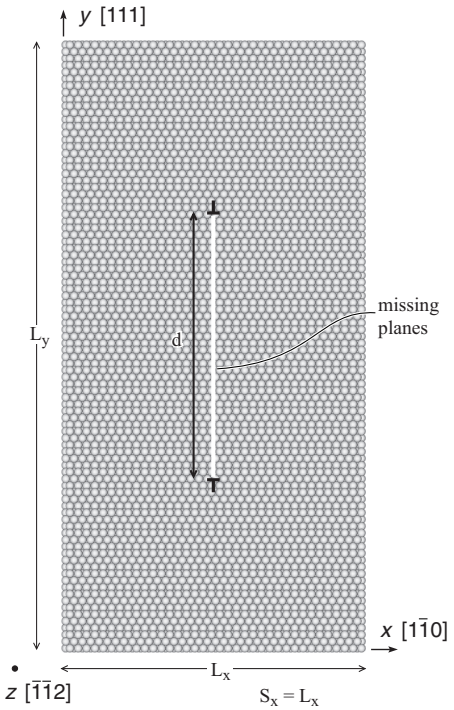

FIG. 1. Geometry for $\beta = 90^\circ$ (edge) dislocation dipoles (dislocation spacing S_x equals system dimension L_x).

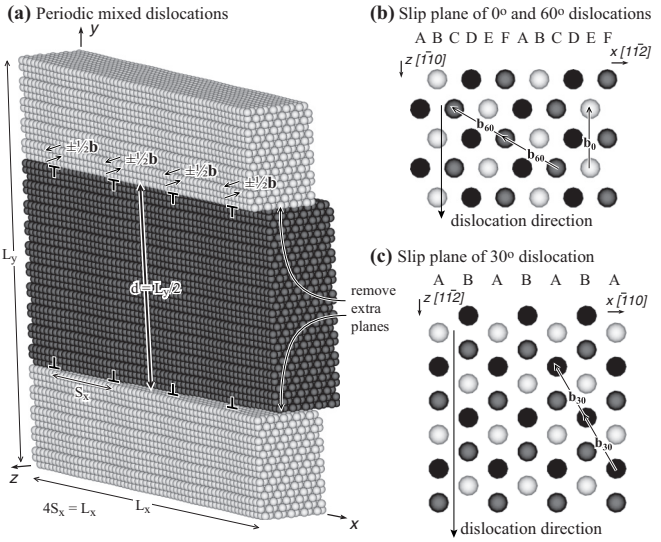

FIG. 2. Geometry for screw and mixed dislocations: (a) Three-dimensional configuration, (b) top view of $\beta = 0^\circ$ (screw) and $\beta = 60^\circ$ (mixed) dislocation slip plane, and (c) top view of $\beta = 30^\circ$ dislocation slip plane.

anisotropic theory (using the MADSUM code [2,20]), allowing for the core energy to be uniquely determined from MD simulations for a given character angle. We use both isotropic and anisotropic theories for these calculations. This is because most discrete dislocation dynamics codes use isotropic theory to compute dislocation interactions and the analytical expressions of isotropic theory allow us to rationalize our results.

A. Edge dislocations ($\beta = 90^\circ$)

The geometry of the method for edge dislocations is shown in Fig. 1. The system has dimensions of L_x, L_y, and L_z in the x, y, and z directions, respectively. When the system is aligned in the $[1\bar{1}0]$ x and $[111]$ y directions, an edge dislocation dipole with a Burgers vector $[1\bar{1}0]a/2$ and a dislocation line parallel to the $[\bar{1}\bar{1}2]z$ direction can be created by removing a $(1\bar{1}0)$ plane or equivalently two $(2\bar{2}0)$ planes as indicated by the white line in Fig. 1. The height of the dipole d equals the height of the missing planes. Under periodic boundary conditions, the dislocations form an infinite array along x and y. Each dislocation has infinite length in the z direction, and the dislocation spacing in the x direction S_x equals the system dimension L_x.

Using this atomistic configuration, we compute the total energy of the system with and without a dislocation dipole present using time-averaged MD simulations (discussed below). Note that the number of atoms in the dislocation-containing system N_d may not equal the number of atoms in the dislocation-free system N_0 due to the missing planes of the edge component of dislocations. Fortunately, each atom in the dislocation-free system is identical, and as a result, the energy of the dislocation-free system can be scaled by a factor of N_d/N_0 to match the number of atoms in the dislocation-containing system. Under this condition, the energy due to the dipole array is the difference in the energies (after the scaling) between these two configurations. As shown in the Appendix, the dipole array energy can be expressed analytically using isotropic linear elasticity theory for a chosen core radius r_0. As discussed in Sec. III C, fitting the MD data to this analytical equation then allows us to determine the core energy [18].

B. Screw ($\beta = 0^\circ$) and mixed dislocations ($0^\circ < \beta < 90^\circ$)

The method described above cannot be applied to screw and mixed dislocations because the shear deformation of the screw component destroys the crystal periodicity. As shown in Fig. 2(a), if the dipole distance is exactly half of the system dimension, i.e., $d = L_y/2$, we can always create a dislocation dipole symmetrically as long as the two half regions (the dark and light regions) are displaced equally by $\pm\frac{1}{2}\mathbf{b}$. Note that we found this symmetrical condition necessary to ensure the correct results. By then introducing multiple dislocation dipoles, we can always satisfy periodic boundary conditions; however, the number of dipoles necessary depends on the character angle of the dislocation lines. As an example, Fig. 2(b) shows a common slip plane for $\beta = 0^\circ$ (screw) and 60° dislocations where the dislocation line aligns with z $[\bar{1}10]$, the screw Burgers vector of $\mathbf{b_0} = [1\bar{1}0]a/2$ forms a $\beta = 180^\circ$ (or equivalently $\beta = 0^\circ$) angle, and the $\beta = 60^\circ$ Burgers vector of $\mathbf{b_{60}} = [0\bar{1}1]a/2$ forms a $\beta = 120^\circ$ (or equivalently $\beta = 60^\circ$) angle. The plane stacking in the x $[11\bar{2}]$ direction is $ABCDEFABCDEF\ldots$. It can be seen that an arbitrary C plane can recover to another C plane if it is shifted by $2\mathbf{b_{60}}$. Hence, periodic boundary conditions can be maintained for the $\beta = 60^\circ$ dislocation if we create four dislocation diploes in the computational cell as shown in Fig. 2(a). Likewise, an arbitrary E plane can recover to another E plane if it is shifted by $\mathbf{b_0}$. Hence, periodic boundary conditions can be used for the screw dislocation

if we create two dislocation dipoles. Similarly, the $\beta = 30°$ dislocation shown in Fig. 2(c) can also be simulated under periodic boundary conditions by creating four dislocation dipoles per cell. Using similar arguments, the character angles 10.89°, 19.11°, 40.89°, 49.11°, 70.89°, and 79.11° can be simulated using 28 dislocation dipoles. These observations allow our method to be extended to screw and mixed dislocations.

The approach described above requires adding more dislocation to the simulation cell, causing the size of the atomistic system to increase. With this approach, all simulation cells are orthorhombic. Although it is possible to reduce the number of dislocations by making the axes of the cell nonorthorhombic [1], we have opted for orthorhombic cells because there is less possibility for artifacts due to improper enforcement of periodicity and/or pressure-free boundary conditions.

C. Time-averaged MD simulations

We have found that, although molecular statics (MS) energy calculations based on the conjugate gradient method can give low relative errors, they produce large total errors that increase as the system dimension increases [18]. This is not satisfactory for calculating dislocation energies, which are related to total energies of (dislocated and perfect) systems if the length along dislocation is fixed. Time-averaged properties of long-time MD simulations, on the other hand, are found to converge satisfactorily regardless of the system dimensions [18]. This sounds surprising at a first sight but can be understood because the time-averaged MD calculations not only average out the thermal noises, but also are analogous to performing ensemble averages of many MS simulations with different perturbations of initial configurations. Additionally, MS pertains only to 0 K whereas finite temperature effects are incorporated in MD. Moreover, finite temperature systems are less likely to become trapped in metastable states, making them more robust for determining the minimum energy core configuration.

The majority of our simulations are performed at 300 K whereas selected other temperatures also are used to explore the temperature effects. All properties presented in this paper are time averaged from 4-ns MD simulations using a time step of 0.004 ps. After discarding the first 0.8 ns to allow for equilibration, the system energy and dimension are averaged over all the time steps for the remaining 3.2 ns. Unless otherwise indicated, our simulations use a zero pressure N-P-T (constant number of atoms, pressure, and temperature) ensemble with the dimension in the dislocation line direction (z) further fixed to match the plane strain assumption used in the classical dislocation theories. We also perform simulations that allow the z dimension to change but the same results are obtained as will be shown below. MD code LAMMPS [21,22] is used for all of our simulations.

III. RESULTS AND DISCUSSION

A. Edge dislocations ($\beta = 90°$)

Two series of simulations are performed. In the first series, the crystal contains 72 $(2\bar{2}0)$ planes in x, 174 (111) planes in y, 30 $(\bar{2}\bar{2}4)$ planes in z, and the dislocation dipole distance d varies from 3 to 171 (111) planes. The same series of simulations are repeated for both 300- and 100-K temperatures. The resulting total dislocation line energies

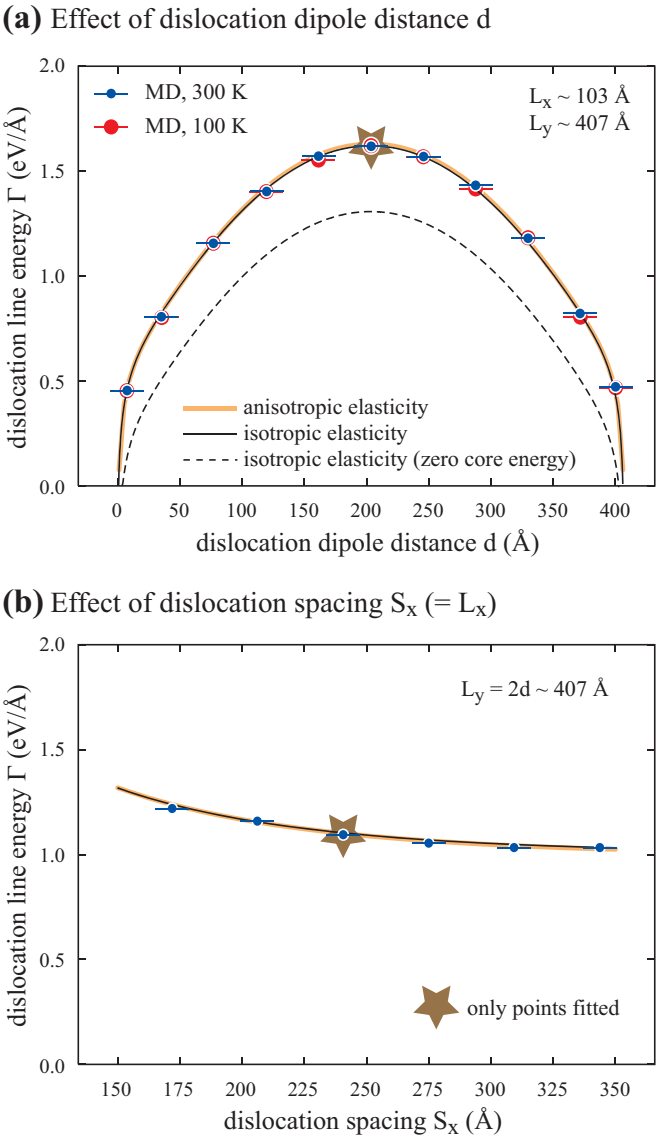

FIG. 3. Edge dislocation line energy as a function of (a) dislocation dipole distance d and (b) dislocation spacing S_x (= L_x). Error bars represent the standard deviation of MD data. Note that in (a), the solid and dashed lines differ only by the constant core energy.

(including both the core and the elastic energies) and their standard deviation are shown as a function of the dipole height in Fig. 3(a). The thin black solid line in the figure corresponds to an isotropic fit to few representative MD data (marked by the brown stars in both Figs. 3 and 4) using Eq. (A1) after selecting an appropriate core radius of $r_0 = 10$ Å. Additionally, we show the fit using anisotropic elasticity theory (with $C_{11} = 118.4$, $C_{12} = 62.6$, and $C_{44} = 33.5$ GPa)[1] as a thick orange solid line. We defer a discussion on the fitting process and the effects of the core radius until later.

[1]These elastic constants differ slightly from the 0 K constants of the interatomic potential ($C_{11} = 114.9$, $C_{12} = 62.6$, and $C_{44} = 31.6$ GPa). We used slightly different values in order to achieve an optimal fit with the MD results which were obtained at 300 K.

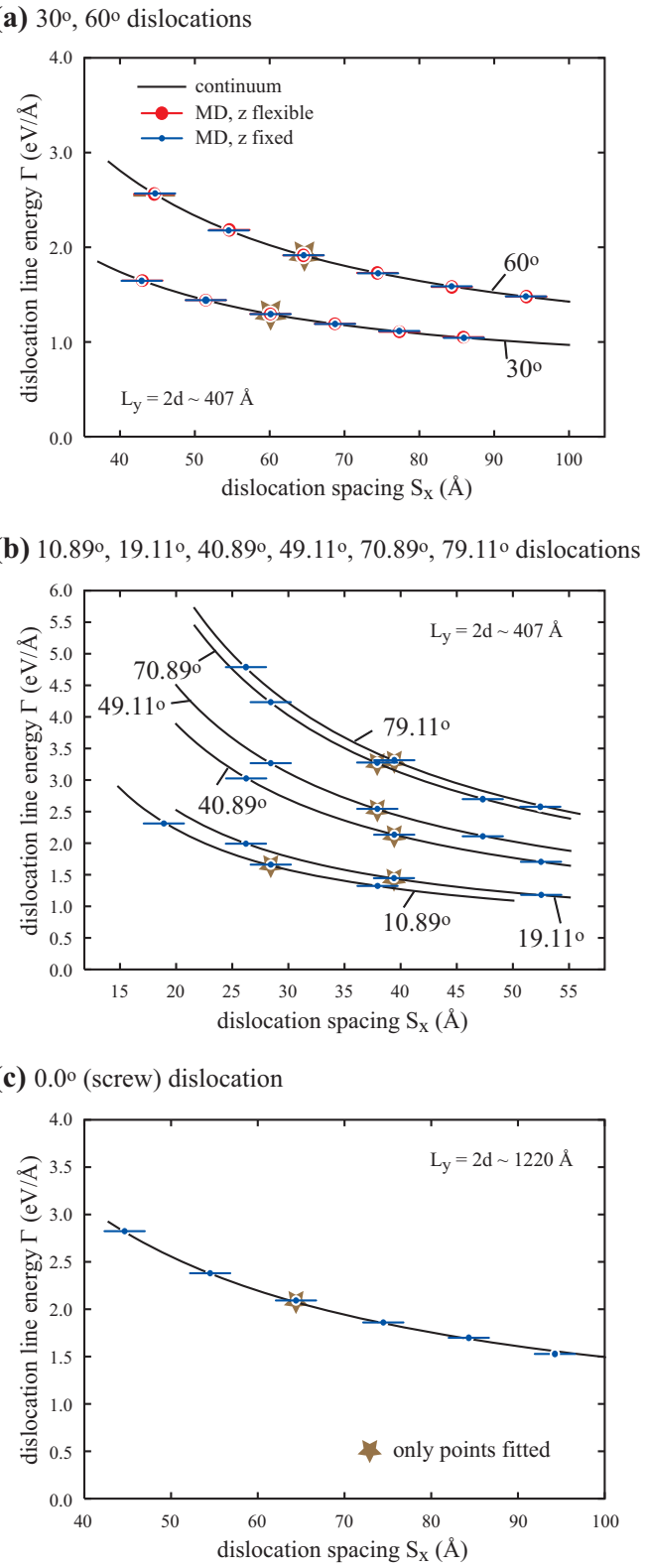

FIG. 4. Line energies as a function of dislocation spacing S_x for (a) 30° and 60°, (b) 10.89°, 19.11°, 40.89°, 49.11°, 70.89°, and 79.11°, and (c) 0° dislocations. Error bars represent the standard deviation of MD data.

It can be seen from Fig. 3(a) that the statistical errors of all of our MD data are near zero within the numerical resolution demonstrated in the figure. A related consequence of the zero errors is that all of our MD data fall right on top of the continuum line, despite the fact that many MD data are not used in the fitting. This strongly validates our MD approach for calculating dislocation energies, which also corroborates well our derived isotropic continuum expressions for periodic dislocation arrays Eqs. (A1)–(A5) in the Appendix. Interestingly, the isotropic curve matches the anisotropic curve perfectly, justifying the validity of the isotropic approach for aluminium analysis. One important observation from Fig. 3(a) is that the temperature does not impact the core energy. This is because differences in entropies and thermal energies between perfect and dislocated systems are both negligible [23].

For reference, the thin black dashed line in Fig. 3(a) is the isotropic continuum result without the core energy. The difference between the thin dashed and the solid lines, corresponding to the constant core energy, is a significant fraction of the overall line energy for the range of dipole configurations considered. Clearly the error caused by ignoring the core energy is significant, demonstrating that our approach is a sensitive method for studying dislocation energies.

Figure 3(a) shows that the dislocation energies are symmetric with respect to dipole height d. This is because when d goes to zero, the dislocations in the dipole annihilate, leading to a low energy. When d is large (close to L_y), dislocations and their other dipole counterparts (periodic images) also annihilate, leading to a low energy. Capturing this phenomenon is one strong validation of our MD data.

The second series of simulations examines the dislocation energy as a function of the lateral spacing S_x of the dislocation dipoles. For this series, the crystal contains 174 (111) planes in y, 30 $(\bar{2}\bar{2}4)$ planes in z, the dislocation dipole distance d equals 87 (111) planes, and the x dimension of the system varies from 120 to 240 $(2\bar{2}0)$ planes. The same method is used to calculate the dislocation energies. The corresponding results are shown in Fig. 3(b) as a function of dislocation lateral spacing $S_x(=L_x)$. Again, Fig. 3(b) indicates that the MD results fit the continuum model (both isotropic and anisotropic) very well.

B. Mixed ($0° < \beta < 90°$) and screw ($\beta = 0°$) dislocations

Mixed dislocations with regular angles $\beta = 60°$ and 30° and nonregular angles $\beta = 10.89°$, 19.11°, 40.89°, 49.11°, 70.89°, and 79.11°, as well as the screw dislocation with $\beta = 0°$, are all studied. For $\beta = 60°$, the crystal contains 174 (111) planes in y, 16 $(2\bar{2}0)$ planes in z, the dislocation dipole distance d equals 87 (111) planes, and the x dimension of the system varies from 216 to 456 $(22\bar{4})$ planes. For $\beta = 30°$, the crystal contains 174 (111) planes in y, 30 $(22\bar{4})$ in z, d equals 87 (111) planes, and the x dimension varies from 120 to 240 $(\bar{2}20)$ planes. Four dislocation dipoles are created in the computational cell as shown in Fig. 2(a) so that the lateral dislocation spacing S_x equals $L_x/4$. The crystals used for dislocations with $\beta = 10.89°$, 49.11°, and 70.89° contain 174 (111) planes in y, 54 $(\frac{9}{7}\frac{36}{7} - \frac{45}{7})$ planes in z, 87 (111) planes for the dislocation dipole height d, and various x dimensions from 1050 to 2625 $(-\frac{45}{7}\frac{30}{7}\frac{15}{7})$ planes. The only difference among the 10.89°, 49.11°, and 70.89° dislocations is that they have different Burger vectors $\mathbf{b} = [01\bar{1}]a/2$, $[\bar{1}01]a/2$, and $[\bar{1}10]a/2$, respectively. For dislocations with $\beta = 19.11°$,

40.89°, and 79.11° angles, the crystals contain 174 (111) planes in y, 45 ($\frac{45}{7} - \frac{30}{7} - \frac{15}{7}$) planes in z, 87 (111) planes for the dislocation dipole height d, and various x dimensions from 1512 to 3024 ($\frac{9}{7}\frac{36}{7} - \frac{45}{7}$) planes. The Burgers vectors for the 19.11°, 40.89°, and 79.11° dislocations correspond to $\mathbf{b} = [\bar{1}10]a/2$, $[\bar{1}01]a/2$, and $[01\bar{1}]a/2$, respectively. Unlike the 60° and 30° regular angle dislocations, the nonregular angles 10.89°, 19.11°, 40.89°, 49.11°, 70.89°, and 79.11° require 28 dislocation dipoles to be used in the computational cell to maintain periodic boundary conditions. As a result, $S_x = L_x/28$. Following the same method as described above, total dislocation line energies are calculated as a function of S_x, and the results are shown in Fig. 4(a) for the regular angles (30° or 60°) and in Fig. 4(b) for the nonregular angles. Again, the MD results are very well characterized by the continuum model.

The $\beta = 0°$ case imposes challenges for fcc metals due to the annihilation of screw dislocations by cross slip. Through extensive iterations, we find that when the y dimension is increased above 522 (111) planes to reduce the attraction between opposite dislocations and when the temperature is reduced below 10 K to trap dislocations in metastable locations, the combination of both conditions can prevent cross slip. Fortunately, the use of a low temperature does not impact the results as has been shown in Fig. 3(a). Hence, we perform simulations at 10 K for the $\beta = 0°$ case using crystals that contain 522 (111) planes in y, 16 ($2\bar{2}0$) planes in z, a dipole height d of 261 (111) planes, and various x dimensions from 108 to 228 ($22\bar{4}$) planes. The results obtained for the 0° dislocations are shown in Fig. 4(c). Again, the data points fall right on top of the continuum line.

The MD simulations discussed above use a fixed z dimension assumed in the dislocation elastic theories (plane strain). We have also performed similar MD simulations where the z dimension is allowed to relax, and the results are included in Fig. 4(a). Interestingly, the flexible z condition produces exactly the same results as the fixed z condition.

C. Dislocation core energies

To compute the core energy using anisotropic theory, we use the cubic elastic constants given above in conjunction with the MADSUM code [2,20]. In the isotropic theory, the continuum expression for the energy of periodic dislocation arrays Eq. (A1) involves four parameters: dislocation core radius r_0, core energy E_c, and elastic constants G and ν. These parameters can be obtained by fitting to the MD data. However, the magnitude of the core radius r_0 is not unique. Conventionally, the only requirement for r_0 is that any region outside r_0 satisfies linear elasticity theory. Obviously, there exists a minimum value $r_0^{\min}$ so that any $r_0 \geqslant r_0^{\min}$ can be taken as a valid core radius. This is because elasticity theory breaks down very near the dislocation core, causing the elastic energy to go to infinity as the core radius goes to zero. Hence, the core radius must be large enough to exclude this unphysical region. On the other hand, the core energy is really just a correction to the linear elastic theory at a given reference core radius r_0. As a result, any value of r_0 (including $r_0 = 0$) can be taken as a valid core radius if the core energy is allowed to be negative. Here we define the minimum value $r_0^{\min}$ so that any $r_0 \geqslant r_0^{\min}$ will always lead to positive core energies for all values of β.

TABLE I. Dislocation core energies E_c^{iso} and E_c^{aniso} (eV/Å) obtained from isotropic and anisotropic elasticity theories for a core radius of $r_0 = 10$ Å.

Dislocation angle β	E_c^{iso}	E_c^{aniso}
00.00°	0.295	0.170
10.89°	0.291	0.197
19.11°	0.296	0.233
30.00°	0.306	0.271
40.89°	0.298	0.254
49.11°	0.308	0.267
60.00°	0.314	0.297
70.89°	0.320	0.293
79.11°	0.316	0.294
90.00°	0.315	0.318

Through trial-and-error fitting, $r_0^{\min}$ is determined to be 2.0 and 2.5 Å for isotropic and anisotropic theories, respectively.

Unlike the curves shown in Figs. 3 and 4 that are fitted to few MD data points, we now fit all MD data to yield the most precise fit. Table I shows our fitted dislocation core energies with $r_0 = 10$ Å obtained for different character angles using both anisotropic and isotropic theories. Fits for different core radii all result in identical isotropic elastic constants of $G = 0.1830\,\text{eV/Å}^3$ (29.3 GPa) and $\nu = 0.3874$, very close to the values of $G = 0.169\,\text{eV/Å}^3$ (27 GPa) and $\nu = 0.34$ commonly cited for aluminium [24],[2] confirming the robustness of our results. Comparing the isotropic and anisotropic core energies, we find that, despite the nearly isotropic behavior of aluminium, the core energies predicted by the two theories are different. For the given core radius, anisotropic theory gives that the core energy varies by nearly a factor of 2 from $\beta = 0°$ to 90° whereas in isotropic theory the core energy is nearly independent of character angle. Note, however, different core energies do not mean that the two theories are inconsistent. In fact, the two theories yield exactly the same total dislocation energies as shown in Fig. 3. The differences just mean that the two theories have different allocations of the total dislocation energies to the core and the elastic components.

To reiterate, our results are strongly validated from numerous aspects: (1) the convergence to a single core energy at different dislocation spacings for a given character angle and a given core radius, (2) the convergence to a single set of isotropic elastic constants for all dislocation spacings, orientations, and core radii, and (3) the strong match between MD results and both the isotropic and the anisotropic continuum results.

D. Analytical expression of core energy as a function of angle β

Using our MD results and isotropic elasticity theory, we can derive an analytical expression for the dislocation core energy

[2]Note that while aluminium is elastically anisotropic like most crystalline solids, it exhibits a relatively weak anisotropy ratio of $A = 1.2$ in both experiments and our potential [19].

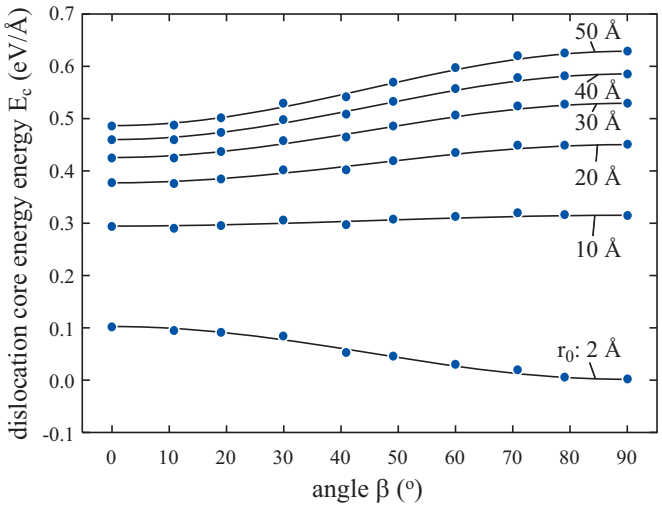

FIG. 5. Dislocation core energies as a function of dislocation angle β at different core radii r_0.

at any character angle and with any core radius. To do so, we make the following assumption: Increases in the core energy as the core radius increases beyond the minimum core radius are due to elastic energy. Hence, the core energy can be written as

$$E_c(r_0,\beta) = E_c^{\text{ref}}(\beta) + \frac{Gb^2}{4\pi}\left(\cos^2\beta + \frac{\sin^2\beta}{1-\nu}\right)\ln\frac{r_0}{r_0^{\text{ref}}}. \quad (2)$$

The first term is the core energy at a reference core radius r_0^{ref} ($r_0^{\text{ref}} \geqslant r_0^{\text{min}}$), and the second term is the change in elastic energy attributed to the core upon changing the core radius from r_0^{ref} to r_0 ($r_0 \geqslant r_0^{\text{min}}$) [25]. Note that the same reasoning could be applied using anisotropic elasticity, however an analytical expression is not readily available. To complete this expression, we need to develop an analytical form for the core energy $E_c^{\text{ref}}(\beta)$ at a chosen reference core radius r_0^{ref}. In principle, $E_c^{\text{ref}}(\beta)$ should depend on crystal structure. For example, in body-centered-cubic materials, screw dislocations have nonplanar cores whereas edge dislocations have planar cores so that these two types of dislocations could have different core energies [26]. Examining our data, however, we find that the $E_c^{\text{ref}}(\beta)$ can be expressed in the same form as the elastic energy [25],

$$E_c^{\text{ref}}(\beta) = A\,\sin^2\beta + B\,\cos^2\beta. \quad (3)$$

For example, if we choose a reference radius of $r_0^{\text{ref}} = 30$ Å, then the parameters $A = 0.5294$ and $B = 0.4528$ eV/Å, which correspond respectively to the edge and screw dislocation core energies derived from the MD simulations described above. In Fig. 5 we plot our core energy data for five core radii between 2 and 50 Å with curves generated using Eqs. (2) and (3) at $r_0^{\text{ref}} = 30$ Å. The figure indicates that the core energies of aluminium very well satisfy Eqs. (2) and (3) for all character angles and core radii; this constitutes the major result of the present paper. We are currently implementing this finding in dislocation dynamics simulation models.

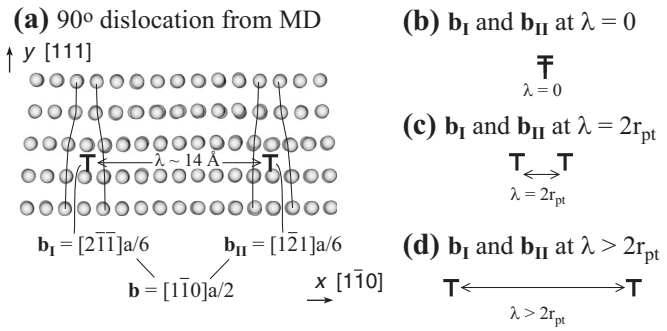

FIG. 6. Dissociated core configuration of a $\beta = 90°$ (edge) dislocation. (a) Front view of the MD configuration, (b) schematic of the perfect dislocation, (c) schematic of the two partials separated by r_{pt}^{min}, and (d) schematic of the two partials separated by λ.

E. Effects of dislocation core structures

We have used elastic energy expressions for perfect dislocations to compute the core energy of a dislocation in a fcc solid that has dissociated into two partial dislocations bounding a stacking fault. Furthermore, we have found that the minimum core radius for this analysis is much smaller than the separation distance between these partial dislocations (shown below). With analysis of the core structure of an isolated dislocation, we can gain further insight into the physics of extended dislocation cores.

The front view (x-y) of the atomic configuration with $\beta = 90°$ (edge) dislocation is examined in Fig. 6(a). As expected, the perfect dislocation with a $\vec{b} = [1\bar{1}0]a/2$ Burgers vector splits into two partials with Burgers vectors of $\vec{b}_I = [2\bar{1}\bar{1}]a/6$ and $\vec{b}_{II} = [1\bar{2}1]a/6$. Because aluminium has a large stacking fault energy of $\eta_{sf} = 133\,\text{mJ/m}^2$ [19], a relatively small separation distance of $\lambda \approx 14$ Å between the two partials is observed. However, this separation distance is significantly larger than the minimum core radius discovered above.

To better understand how the energetics of the dissociated structure relates to our results, we compute the energy change when a perfect edge dislocation dissociates into two partials (similar to the approach used in Ref. [27]). Since we are focusing on the core structure, we only consider an isolated extended dislocation in an infinite medium (rather than periodic arrays of dislocations, such as we did above). The line energy of a perfect edge dislocation in isotropic elasticity can be stated as [25]

$$\Gamma_{pf} = E_{c,pf}(r_{pf},\beta = 90°) + \frac{Gb^2}{4\pi(1-\nu)}\ln\frac{R}{r_{pf}}, \quad (4)$$

where the subscript pf denotes a perfect dislocation, $E_{c,pf}(r_{pf},\beta = 90°)$ is the core energy associated with the core radius r_{pf}, and R is the outer cutoff radius. The energy change $\Delta\Gamma$ when the two partials move apart is the work performed by the stress fields of the partials plus the energy of the stacking fault. To compute these quantities, we consider two stages of separation. First, the separation distance of the two partials increases from $\lambda = 0$ to $\lambda = 2r_{pt}$ as shown in Figs. 6(b) and 6(c), where r_{pt} is the core radius of a partial dislocation so that $2r_{pt}$ is the overlap region of the two partial

dislocation cores. During this stage of separation we lump all of the work performed into a change in the core energy, leading to an energy change in [18]

$$\Delta\Gamma_1 = (2E_{c,pt} + 2r_{pt}\eta_{sf}) - E_{c,pf}, \tag{5}$$

i.e., the core energy of the perfect dislocation $E_{c,pf}$ is replaced by the core energies of two partials $2E_{c,pt}$ plus a stacking fault energy (η_{sf} refers to the stacking fault energy per unit of area). The work performed to further separate the two partials from $\lambda = 2r_{pt}$ to $\lambda > 2r_{pt}$ as shown in Figs. 6(c) and 6(d) can be obtained from linear elasticity [18]. Adding in the energy from the stacking fault then gives an energy change in

$$\Delta\Gamma_2 = \frac{Gb^2}{8\pi}\left(\frac{1}{3} - \frac{1}{1-\nu}\right)\ln\frac{\lambda}{2r_{pt}} + \left(\lambda - 2r_{pt}\right)\eta_{sf}. \tag{6}$$

Hence, the total energy difference between the dissociated dislocation Fig. 6(d) and the perfect dislocation Fig. 6(b) can be expressed as

$$\Delta\Gamma = \Delta\Gamma_1 + \Delta\Gamma_2 = 2E_{c,pt} - E_{c,pf} + \frac{Gb^2}{8\pi}\left(\frac{1}{3} - \frac{1}{1-\nu}\right)\ln\frac{\lambda}{2r_{pt}} + \lambda\eta_{sf}. \tag{7}$$

If we assume $r_{pt} = 1.0$, $b = 2.8634$ Å and use the corresponding parameters mentioned above, the elastic and stacking fault components give $\frac{Gb^2}{8\pi}(\frac{1}{3} - \frac{1}{1-\nu})\ln\frac{\lambda}{2r_{pt}} + \lambda\eta_{sf} = -0.0345\,\text{eV/Å}$. The negative value drives the dissociation of the perfect dislocation.

The total line energy of the extended dislocation is now $\Gamma = \Gamma_{pf} + \Delta\Gamma$. Using Eqs. (4) and (7) and after some manipulation, we have that

$$\Gamma = 2E_{c,pt} + \frac{Gb^2}{8\pi}\left[\left(\frac{1}{3} - \frac{1}{1-\nu}\right)\ln\frac{\lambda}{2r_{pt}} + \frac{2}{1-\nu}\ln\frac{r_{pt}}{r_{pf}}\right] + \lambda\eta_{sf} + \frac{Gb^2}{4\pi(1-\nu)}\ln\frac{R}{r_{pt}}. \tag{8}$$

Only the last term contributes to the long-range elastic component of the line energy, so we recognize that the core energy we have computed and given in Table I corresponds to the remaining terms,

$$E_c = 2E_{c,pt} + \frac{Gb^2}{8\pi}\left[\left(\frac{1}{3} - \frac{1}{1-\nu}\right)\ln\frac{\lambda}{2r_{pt}} + \frac{2}{1-\nu}\ln\frac{r_{pt}}{r_{pf}}\right] + \lambda\eta_{sf}. \tag{9}$$

This analysis demonstrates the connection between the line energy expression for a perfect dislocation and the line energy expression for an extended dislocation. Note that comparing the long-range elastic interaction terms in Eqs. (4) and (8) shows that r_{pf} is equivalent to r_{pt}, meaning that the minimum core radius we have obtained with our atomistic computations actually corresponds to the minimum core radius of the partial dislocations rather than the overall extended dislocation. This explains why we find a minimum core radius that is much smaller than the separation distance between the partials.

IV. CONCLUSIONS

A robust MD model has been developed to calculate the core energies of mixed dislocations. This model does not require continuum boundary conditions, is applicable for the full character angle range of $0^\circ \leqslant \beta \leqslant 90^\circ$, produces strongly convergent results, and is constructed from orthorhombic systems under the plane strain condition consistent with the classical dislocation theories. Based on a high-fidelity bond order potential, we have used this model to study dislocation core energies of aluminium as a function of dislocation angle β. The following conclusions have been obtained:

(1) Although dislocations are dissociated, the apparent (mathematical) dislocation core radius in aluminium is as small as $r_0 = 2.0$ Å with isotropic elasticity theory and 2.5 Å with anisotropic elasticity theory, despite the fact that the extended core has a width of greater than 14 Å. This is because the core radius pertains to the partial dislocations in the core.

(2) Values of $r_0 > 2.0$ Å can also be used. A larger radius in general leads to a larger core energy. In particular, the increase in core energy always equals the elastic strain energy of the added volume due to the increase in the core radius.

(3) In isotropic elasticity theory, dislocation core energy as a function of character angle satisfies an expression of the form $E_c(\beta) = A\sin^2\beta + B\cos^2\beta$, which is similar to the elastic energy.

(4) Dislocation energies are independent of temperature over the temperature range considered here (100–300 K).

ACKNOWLEDGMENTS

Sandia National Laboratories is a multiprogram laboratory managed and operated by Sandia Corporation, a wholly owned subsidiary of Lockheed Martin Corporation, for the U.S. Department of Energy's National Nuclear Security Administration under Contract No. DE-AC04-94AL85000. This work was performed under the Laboratory Directed Research and Development (LDRD) Project No. 165724.

APPENDIX: DISLOCATION ENERGY UNDER PERIODIC BOUNDARY CONDITIONS

Following the previous approach for edge dislocations [18], the dislocation line energy Γ for periodic mixed dislocations with a mixed angle β can be derived as

$$\Gamma = E_c + \frac{Gb^2}{4\pi(1-\nu)}\cos^2\alpha + \sin^2\beta E_{0,\text{edge}} + \cos^2\beta E_{0,\text{screw}} + 2\sin^2\beta\sum_{i=1}^{\infty}E_{i,\text{edge}} + 2\cos^2\beta\sum_{i=1}^{\infty}E_{i,\text{screw}}, \tag{A1}$$

where

$$E_{0,\text{edge}} = \frac{Gb^2}{4\pi(1-\nu)}\left\{\ln\left(\frac{d}{r_0}\right) + \ln\left(\frac{L_y-d}{L_y}\right) - \ln\left[Ga\left(\frac{L_y+d}{L_y}\right)\right] - \ln\left[Ga\left(2-\frac{d}{L_y}\right)\right]\right\}, \tag{A2}$$

$$E_{0,\text{screw}} = \frac{Gb^2}{4\pi}\left\{\ln\left(\frac{d}{r_0}\right) + \ln\left(\frac{L_y-d}{L_y}\right) - \ln\left[Ga\left(\frac{L_y+d}{L_y}\right)\right] - \ln\left[Ga\left(2-\frac{d}{L_y}\right)\right]\right\}, \tag{A3}$$

$$E_{i,\text{edge}} = \frac{Gb^2}{8\pi(1-\nu)}\left\{\frac{4\pi i S_x \coth\left(\frac{\pi i S_x}{L_y}\right)\sin^2\left(\frac{\pi d}{L_y}\right)}{L_y\cosh\left(\frac{2\pi i S_x}{L_y}\right) - L_y\cos\left(\frac{2\pi d}{L_y}\right)} + \ln\left[\cos^2\left(\frac{\pi d}{L_y}\right) + \coth^2\left(\frac{\pi i S_x}{L_y}\right)\sin^2\left(\frac{\pi d}{L_y}\right)\right]\right\}, \tag{A4}$$

$$E_{i,\text{screw}} = \frac{Gb^2}{8\pi}\ln\left[\cos^2\left(\frac{\pi d}{L_y}\right) + \coth^2\left(\frac{\pi i S_x}{L_y}\right)\sin^2\left(\frac{\pi d}{L_y}\right)\right]. \tag{A5}$$

In Eqs. (A1)–(A5), E_c and r_0 are the core energy and core radius of an isolated dislocation, Ga is a Euler γ function, coth and cosh are hyperbolic functions, G is the shear modulus, ν is Poisson's ratio, b is Burgers magnitude, α is an angle measuring the dislocation dipole direction (in particular, $\alpha = 0^\circ$ means vertical dislocation dipole studied in the present paper, and $\alpha = 90^\circ$ means horizontal dislocation dipole), S_x is dislocation separation distance in x, L_y is periodic length in y, and d is dislocation dipole height. Note that Eqs. (A1)–(A3) involve numerous changes compared to the previous work [18]. First, the core radius r_0 defined here is equivalent to $2r_0$ defined previously [18]. Second, there is a constant $\frac{Gb^2}{4\pi(1-\nu)}\cos^2\alpha$ in Eq. (A1) that is counted as elastic contribution whereas in the previous work this constant term is lumped into the core energy. These two modifications have a zero impact on the model because they do not change the total energy of dislocations; they only change the definition of dislocation core radius and core energy. We modify these definitions so that they are consistent with Hirth and Lothe [25]. Finally, the second term in the curly braces "{ }" of the right-hand side of Eqs. (A2) and (A3) is now expressed as $\ln(\frac{L_y-d}{L_y})$ whereas it was expressed as $\ln(\frac{L_y-d}{L_y-2r_0})$ in the previous work [18]. The new expression is more rigorous, but the effect is negligible because $L_y \gg r_0$.

Even Eq. (A1) does not have a closed form; it converges very fast so that the error is negligible if a few terms (say 20) are included (in the present paper, we included 100 terms). We also wish to point out that Fourier methods can also be used to compute the energies of dipolar dislocation arrays [28,29].

[1] V. V. Bulatov and W. Cai, *Computer Simulations of Dislocations* (Oxford University Press, London, 2006).
[2] W. Cai, V. V. Bulatov, J. Chang, J. Li, and S. Yip, Philos. Mag. **83**, 539 (2003).
[3] W. Cai, V. V. Bulatov, J. Chang, J. Li, and S. Yip, Phys. Rev. Lett. **86**, 5727 (2001).
[4] J. Li, C. Z. Wang, J. P. Chang, W. Cai, V. V. Bulatov, K. M. Ho, and S. Yip, Phys. Rev. B **70**, 104113 (2004).
[5] M. Heggie, R. Jones, and A. Umerski, Philos. Mag. A **63**, 571 (1991).
[6] R. Jones, A. Umerski, P. Sitch, M. I. Heggie, and S. Öberg, Phys. Status Solidi A **137**, 389 (1993).
[7] A. S. Nandedkar and J. Narayan, Philos. Mag. A **61**, 873 (1990).
[8] U. Trinczek and H. Teichler, Phys. Status Solidi A **137**, 577 (1993).
[9] A. Aslanides and V. Pontikis, Comput. Mater. Sci. **10**, 401 (1998).
[10] J. R. K. Bigger, D. A. McInnes, A. P. Sutton, M. C. Payne, I. Stich, R. D. King-Smith, D. M. Bird, and L. J. Clarke, Phys. Rev. Lett. **69**, 2224 (1992).
[11] S. Ismail-Beigi and T. A. Arias, Phys. Rev. Lett. **84**, 1499 (2000).
[12] G. Wang, A. Strachan, T. Cagin, and W. A. Goddard, III, Phys. Rev. B **67**, 140101(R) (2003).
[13] J. Bennetto, R. W. Nunes, and D. Vanderbilt, Phys. Rev. Lett. **79**, 245 (1997).
[14] N. Lehto and S. Öberg, Phys. Rev. Lett. **80**, 5568 (1998).
[15] X. Blase, K. Lin, A. Canning, S. G. Louie, and D. C. Chrzan, Phys. Rev. Lett. **84**, 5780 (2000).
[16] E. Clouet, L. Ventelon, and F. Willaime. Phys. Rev. Lett. **102**, 055502 (2009).
[17] G. Lu, N. Kioussis, V. V. Bulatov, and E. Kaxiras, Mater. Sci. Eng., A **309**, 142 (2001).
[18] X. W. Zhou, D. K. Ward, J. A. Zimmerman, J. L. Cruz-Campa, D. Zubia, J. E. Martin, and F. van Swol, J. Mech. Phys. Solids **91**, 265 (2016).
[19] X. W. Zhou, D. K. Ward, and M. E. Foster, J. Alloys Compd. **680**, 752 (2016).
[20] The MADSUM code is available at http://micro.stanford.edu/~caiwei/Forum/2004-08-08-MadSum
[21] S. Plimpton, J. Comput. Phys. **117**, 1 (1995).
[22] The LAMMPS download site, lammps.sandia.gov.
[23] A. H. Cottrell, *Dislocations and Plastic Flow in Crystals* (Oxford University Press, London, 1953).
[24] R. L. Norton, *Machine Design* (Pearson-Prentice Hall, Upper Saddle River, NJ, 2006).
[25] J. P. Hirth, and J. Lothe, *Theory of Dislocations* (McGraw-Hill, New York, 1968).
[26] V. Vitek, Cryst. Lattice Defects **5**, 1 (1974).
[27] T. Tsuru and D. C. Chrzan, Sci. Rep. **5**, 8793 (2015).
[28] T. Mura, Proc. R. Soc. London, Ser. A **280**, 528 (1964).
[29] M. S. Daw, Comput. Mater. Sci. **38**, 293 (2006).